

# Comprehensive characterization and analysis of hexagonal boron nitride on sapphire

Cite as: AIP Advances **11**, 055008 (2021); <https://doi.org/10.1063/5.0048578>

Submitted: 23 March 2021 • Accepted: 16 April 2021 • Published Online: 07 May 2021

S. Saha, A. Rice, A. Ghosh, et al.

## COLLECTIONS

Paper published as part of the special topic on [Materials Science](#)



View Online



Export Citation



CrossMark

## ARTICLES YOU MAY BE INTERESTED IN

[Point defects in two-dimensional hexagonal boron nitride: A perspective](#)

Journal of Applied Physics **128**, 100902 (2020); <https://doi.org/10.1063/5.0021093>

[MOVPE of GaN-based mixed dimensional heterostructures on wafer-scale layered 2D hexagonal boron nitride—A key enabler of III-nitride flexible optoelectronics](#)

APL Materials **9**, 061101 (2021); <https://doi.org/10.1063/5.0049306>

[Thermally annealed wafer-scale h-BN films grown on sapphire substrate by molecular beam epitaxy](#)

Applied Physics Letters **116**, 142104 (2020); <https://doi.org/10.1063/5.0002101>

AIP Advances  
Mathematical Physics Collection

READ NOW





# Comprehensive characterization and analysis of hexagonal boron nitride on sapphire

Cite as: AIP Advances 11, 055008 (2021); doi: 10.1063/5.0048578

Submitted: 23 March 2021 • Accepted: 16 April 2021 •

Published Online: 7 May 2021



S. Saha,<sup>1</sup> A. Rice,<sup>2</sup> A. Ghosh,<sup>1</sup> S. M. N. Hasan,<sup>1</sup> W. You,<sup>1</sup> T. Ma,<sup>3</sup>  A. Hunter,<sup>3</sup>  L. J. Bissell,<sup>4</sup>  R. Bedford,<sup>4</sup> M. Crawford,<sup>2</sup> and S. Arafin<sup>1,a)</sup> 

## AFFILIATIONS

<sup>1</sup>Department of Electrical and Computer Engineering, The Ohio State University, Columbus, Ohio 43210, USA

<sup>2</sup>Sandia National Laboratories, P.O. Box 5800, Albuquerque, New Mexico 87185, USA

<sup>3</sup>University of Michigan, Ann Arbor, Michigan 48109, USA

<sup>4</sup>Materials and Manufacturing Directorate, Air Force Research Laboratory, WPAFB, Ohio 45434, USA

<sup>a)</sup>Author to whom correspondence should be addressed: arafin.1@osu.edu

## ABSTRACT

Hexagonal boron nitride (h-BN) is considered as one of the most promising materials for next-generation quantum technologies. In this paper, we report bulk-like multilayer h-BN epitaxially grown using a carbon-free precursor on c-plane sapphire with a strong emphasis on material characterization and analysis. In particular, structural, morphological, and vibrational properties, and chemical bonding of such van der Waals materials are presented. Between as-grown h-BN and c-plane sapphire, a compressive residual strain induced by both lattice mismatch and thermal expansion mismatch is examined by both theoretical and experimental studies. Atomic force microscopy revealed and scanning electron microscopy supported the presence of wrinkles across the entire surface of the film, likely due to biaxial compressive strain further verified by Raman spectroscopy. Stacking orders in h-BN with a clearly layered structure were confirmed by high resolution transmission electron microscopy, showing that the films have crystallographic homogeneity. Chemical analysis of the as-grown films was done by x-ray photoelectron spectroscopy, which confirmed the formation of stoichiometric h-BN films with excellent uniformity. This wafer-scale chemical vapor deposition-grown layered h-BN with 2D morphology facilitates applications in the fields of quantum- and deep ultraviolet-photonics.

© 2021 Author(s). All article content, except where otherwise noted, is licensed under a Creative Commons Attribution (CC BY) license (<http://creativecommons.org/licenses/by/4.0/>). <https://doi.org/10.1063/5.0048578>

## I. INTRODUCTION

The ultra-wide bandgap semiconductor ( $\sim 6$  eV) h-BN is an important van der Waals (vdW) material and has currently attracted tremendous attention because of its high thermal conductivity ( $2000 \text{ W m}^{-1} \text{ K}^{-1}$ ),<sup>1,2</sup> excellent thermal stability,<sup>3</sup> the presence of a sharp zero phonon line (ZPL),<sup>4</sup> and large Debye-Waller factor.<sup>5</sup> The  $sp^2$ -hybridized bonding makes the material atomically smooth and free from dangling bonds, which support its potential use as an active material for future electronic and optoelectronic devices.<sup>6</sup> This material and its associated point defects are emerging to host the brightest room-temperature single-photon emitters (SPEs), serving as a versatile source of quantum light with unique capabilities for integration in scalable nanophotonic structures.<sup>7</sup> In addition, it also finds applications as electron blocking layers in *p-i-n* devices,<sup>8</sup>

membranes,<sup>9</sup> and flexible electronic devices.<sup>10</sup> The majority of the aforementioned applications of h-BN depend mostly on the successful growth of large-area, single-crystalline, and defect-free h-BN.

There have been extensive efforts to realize large-area and single-crystalline h-BN materials by chemical vapor deposition (CVD),<sup>11</sup> metalorganic CVD (MOCVD),<sup>12,13</sup> and molecular beam epitaxy (MBE).<sup>14</sup> It is a commonly held belief that a growth temperature of  $>1400^\circ\text{C}$  is essential to obtain highly crystalline h-BN.<sup>15</sup> Among several growth technologies, wafer-scale growth of h-BN by CVD is not attractive due to the limited diameter of a horizontal tube furnace and strict requirements in terms of using light-absorbing catalytic metal substrates.<sup>12,16</sup> Although accommodating this high growth temperature requirement is often challenging and sometimes beyond the capability of a conventional reactor, high-quality h-BN on sapphire has been reported at an ultrahigh

temperature in customized MBE where the temperature can reach up to 1600 °C.<sup>14</sup> MOCVD is a popular tool for commercial growth of large-scale h-BN on semiconductor or insulator substrates due to its high-throughput capability.

Since the first demonstration of high-quality h-BN grown by MOCVD,<sup>17</sup> this vdW material has emerged as one of the exciting platforms for making a wide range of next-generation devices. As a substrate material, sapphire is a low-electrical-conductivity choice for MOCVD-grown h-BN films when compared to other catalytic transition metal substrates, such as Ni.<sup>18</sup> Epitaxial growth of BN films on sapphire using MOCVD by introducing an AlN buffer layer has been reported in Ref. 19. AlN-buffer-free h-BN growth was also attempted, and a reasonable crystalline quality was achieved through optimized growth techniques.<sup>20</sup> Despite significant growth efforts made in the past decade toward obtaining good material quality, systematic characterization study on structural, morphological, vibrational, and optical properties as well as chemical bonding of h-BN-on-sapphire is still scarce.

This paper reports wafer-scale two-dimensional (2D) layered single-crystal CVD-grown h-BN films on sapphire substrates in a MOCVD reactor. Although the most commonly used precursor for this process is a combination of triethylborane [(C<sub>2</sub>H<sub>5</sub>)<sub>3</sub>B] and ammonia, (C<sub>2</sub>H<sub>5</sub>)<sub>3</sub>B acts as a possible source of carbon impurities and ammonia also reacts aggressively with substrate and chamber components at a high temperature. For reducing carbon impurities, diborane (B<sub>2</sub>H<sub>6</sub>) with ammonia and borazine (B<sub>3</sub>H<sub>6</sub>N<sub>3</sub>) are the potential precursor candidates. B<sub>2</sub>H<sub>6</sub> is one of the finest choices for growing high-purity BN films as it does not contain Cl, Br, and C atoms in the raw material.<sup>21,22</sup>

The h-BN film described in our study was deposited with B<sub>3</sub>H<sub>6</sub>N<sub>3</sub> as the sole precursor. B<sub>3</sub>H<sub>6</sub>N<sub>3</sub> has been rigorously used earlier for h-BN synthesis on catalytic substrates.<sup>18,23</sup> Previous studies have also confirmed the successful demonstration of h-BN growth on sapphire substrates using the same precursor, which decomposes from ammonia borane.<sup>24,25</sup> The true potential of h-BN and significant advancements in the high-quality material growth can only be leveraged when extensive post-growth characterization and detailed analysis are conducted, which eventually improve the prospects for the nascent device applications beyond quantum emitters. Hence, it is important to thoroughly characterize and analyze the h-BN films through microscopic and spectroscopic studies. This experimental study and in-depth analysis not only provide a fundamental understanding of the morphological, structural, and vibrational properties of such h-BN films, but also provide several new material insights and chemical properties, paving the way for the development of quantum technologies.

## II. EXPERIMENTAL SECTION

Films of h-BN were grown on c-plane sapphire substrates in a vertical, cold-walled, radio frequency (RF)-heated MOCVD reactor. Since this film was deposited with non-metalorganic borazine, the growth process taking place during material deposition is principally CVD-like. Prior to growth, sapphire substrates were etched *in situ* at 1100 °C and 500 Torr total pressure in a 1:1 mixture of flowing H<sub>2</sub> and N<sub>2</sub> for 20 min. The material was grown at 1500 °C and 50 Torr total pressure with N<sub>2</sub> as the diluent and carrier

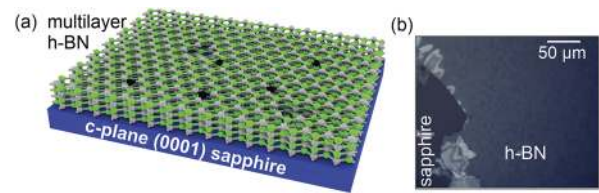


FIG. 1. (a) Schematic diagram of multilayer h-BN thin films grown on c-plane sapphire substrates and (b) Nomarski microscopy image of the sample edge.

gas. B<sub>3</sub>H<sub>6</sub>N<sub>3</sub> partial pressure and flow were held at 130 μTorr and 1.9 μmol/min, respectively, during 3 h of growth. Figure 1 shows a schematic and a Nomarski microscopy image of the multilayer h-BN sample.

The morphological, structural properties, and chemical composition of h-BN thin films were ascertained using various characterization techniques. To determine the crystal structures of the samples, x-ray diffraction (XRD) measurements were carried out on a Bruker D8 Advance diffractometer using a Cu Kα1 radiation source ( $\lambda = 1.5406 \text{ \AA}$ ) equipped with a LYNXEYE XE detector. The XRD system operates at a wavelength of 1.5406 Å to evaluate the crystallinity and determine the c-axis lattice parameter. The system has a line source diffractometer operated in a symmetric reflection mode. A Zeiss Ultra Plus standard detector scanning electron microscopy (SEM) system, at accelerating voltages of 2 and 3 kV, was used to determine the morphology of the h-BN films. The brightness and contrast of the SEM images were linearly adjusted in ImageJ. The pseudo color was added using the ImageJ Gem lookup table to enhance the image visibility. Further morphological analyses were performed in a Bruker Dimension Icon atomic force microscope (AFM). The vibrational characteristics of the h-BN thin films were determined using a Renishaw Raman IR microprobe with an inVia confocal Raman microscope at 514 nm laser excitation wavelength.

X-ray photoelectron spectroscopy (XPS) was performed on the sample to analyze the impact of growth parameters on the chemical structure of the resulting films. All spectra were collected using a Kratos Axis Ultra XPS instrument with a monochromatic Al-Kα source (1486.6 eV, 12 kV, 10 mA) positioned at 53.5° with respect to the sample normal and a beam spot size of 300 × 700 μm<sup>2</sup>. A charge neutralizer was utilized at 1.7 A, 1.5 V, and a charge balance of 2.6 V. Binding energies were calibrated using carbon C 1s peaks at 284.9 eV. Low-resolution survey spectra were acquired using a pass energy of 80 eV with a 1 eV step size, while high-resolution core level scans were collected using a pass energy of 20 eV and steps of 0.1 eV. All data were analyzed and fitted using CasaXPS software (version 2.3.23). All high-resolution spectra were fitted with either a Shirley or linear background, and a Lorentzian (30%)–Gaussian (70%) line shape.

High resolution transmission electron microscopy (HRTEM) was carried out on a JEOL 3100R05 double-corrected STEM operated at 300 kV. The spherical aberration (Cs) of the objective lens was tuned to around −10 μm to obtain optimal high resolution contrast. Electron energy-loss spectroscopy (EELS) was performed using a Gatan Quantum 969 GIF equipped with a K2 direct electron camera.

### III. RESULTS AND DISCUSSIONS

#### A. XRD study

Direct CVD growth of h-BN on sapphire is challenging as it may lead to different polymorphisms including amorphous BN (a-BN), wurtzite BN (w-BN), explosion BN (e-BN), rhombohedral BN (r-BN), turbostratic BN (t-BN), and cubic BN (c-BN).<sup>26</sup> Standard  $2\theta/\omega$  scan of Fig. 2(a) reveals two peaks at around  $26.7^\circ$  and  $41.7^\circ$ , which correspond to (0002) h-BN and the (0006) sapphire crystal planes, respectively, with no other visible peaks.<sup>27</sup> It should be noted that no AlN peaks were found by XRD, and this suggests that nitridation of the sapphire substrate did not occur in the early stage of our growth. The measured c-axis lattice constant is  $6.7 \text{ \AA}$ , which is close to the bulk h-BN value of  $6.67 \text{ \AA}$ .<sup>28</sup> The 0.7% increase in the c-axis lattice constant could be attributed to a residual strain, which is thought to occur from the cooling process after the growth and it will be discussed in AFM study. The slight increase could also imply almost no presence of the undesired t-phase of BN. This may be because of the growth temperature of as low as  $1500^\circ\text{C}$  and/or the pressure of borazine may not be high enough to crystallize BN into a perfect hexagonal phase.

Figure 2(b) presents the x-ray rocking curve of the (0002) diffraction peak of the same h-BN films. The full width at half maximum (FWHM) value of the curve was measured to be  $6660 \text{ arc sec}$ . The observed linewidth is an order of magnitude broader than the previously reported XRD results with a value of  $\sim 385 \text{ arc sec}$ .<sup>29,30</sup> However, this broadened linewidth of our films, possibly occurring due to wrinkling, does not provide a true representation of the film quality. In other words, the high FWHM does not signify that the h-BN materials are crystallographically defective because broadening occurs when some portions of the (0002) planes are not parallel to each other. A detailed discussion on wrinkling is given in the AFM and SEM sections.

#### B. SEM study

To analyze the surface morphology, we performed SEM imaging. Figure 3(a) shows the top-view SEM image of the as-grown h-BN films, which also confirms the presence of the wrinkles in the films. Appearance of wrinkles is common when a vdW material is under in-plane strain. These wrinkles also occur when h-BN with a smaller in-plane lattice constant is grown on a relatively compliant substrate like sapphire. Apart from the wrinkles, SEM also confirmed the presence of the hillocks across the sample surface as evidenced by Fig. 3(b).

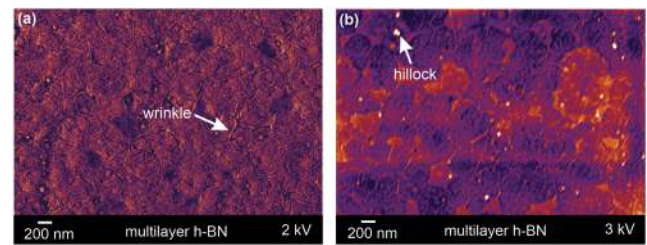


FIG. 3. SEM images of h-BN films, showing (a) wrinkles and (b) hillocks across the surface.

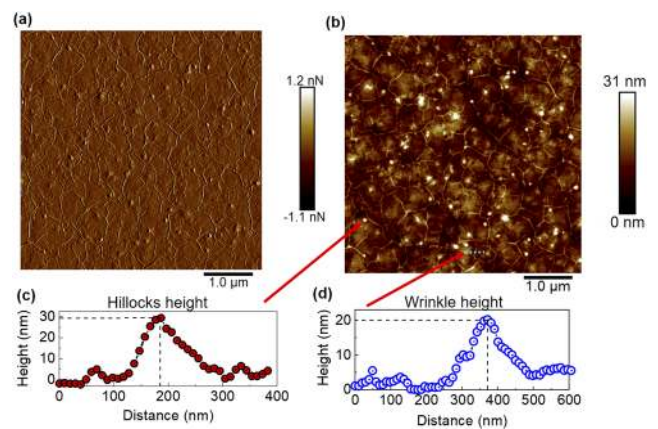


FIG. 4. AFM images of h-BN films under (a) peak force and (b) height scans. The height of the (c) hillocks and (d) wrinkles are also shown.

#### C. AFM study

Figures 4(a) and 4(b) show the AFM images of the surface morphology of our h-BN films with a scan area of  $5 \times 5 \mu\text{m}^2$ . A number of wrinkles across the surface are seen, and the measured height of the wrinkle is around  $20 \text{ nm}$ . Figure 4(c) shows the heights of the wrinkles with a lateral dimension of around  $200 \text{ nm}$ . Appearance of localized wrinkles is a key signature of a strained film.<sup>31</sup> This was also observed from the MOCVD-grown h-BN sample with a thickness of  $30 \text{ nm}$ .<sup>32</sup> The absence of strong interfacial interactions between films and underlying substrates, in general, leads to wrinkles, which may initiate from the defects on the interface between the film and substrates.

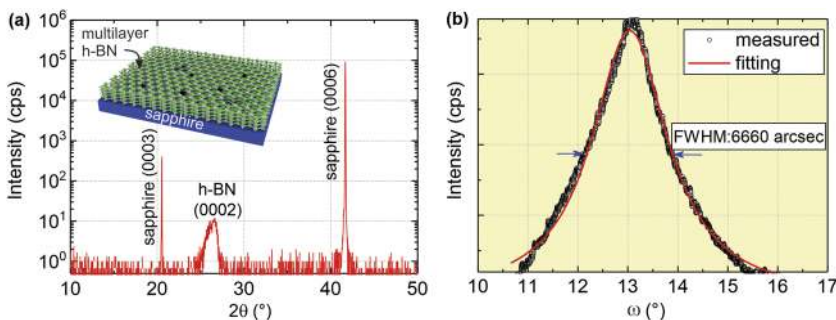


FIG. 2. (a) XRD pattern of single crystalline h-BN films grown on sapphire and (b) rocking curve of the (0002) reflection.

Formation of wrinkles depends on various parameters, such as substrate and film thicknesses, as well as elasticity. Kinetics of the wrinkling control the overall strain distribution across the surface, which could be influenced by the Lennard-Jones interaction. This is used to describe weak vdW potential and Pauli's repulsive potential, which cause pinning of the grown film with the underlying substrate at a high growth temperature.<sup>33</sup> Although the film has a tendency to expand when the system returns to room temperature after growth, the pinned boundaries do not allow the film to expand laterally. As a result, residual strain is induced, which causes wrinkle formation. The wrinkles may also come from isotropic biaxial compressive strain resulting from a thermal expansion coefficient (TEC) mismatch between sapphire and h-BN.<sup>34</sup> As a result, a cooling process from a high growth temperature introduces compressive strain, yielding a release of energy in the form of wrinkles, which creates the roughness in the sample. The root mean square (rms) roughness of the sample was found to be 3.9 nm, which is in good agreement with the previously reported results.<sup>31</sup> This residual strain  $\Delta\varepsilon$  due to the variation in the temperature can be mathematically expressed as

$$\Delta\varepsilon = \int_{RT}^{T_G} \alpha_{\text{h-BN}}(T) - \alpha_{\text{sapphire}}(T) dT, \quad (1)$$

where  $T_G$  and  $RT$  are the growth temperature (1500 °C) and room temperature (27 °C), respectively. The linear thermal expansion coefficients of h-BN and the substrate are denoted as  $\alpha_{\text{h-BN}}$  and  $\alpha_{\text{sapphire}}$ . We used  $\alpha_{\text{h-BN}}(T) = (1.91 \times 10^{-9}T - 2.96 \times 10^{-6})^\circ\text{C}^{-1}$  and  $\alpha_{\text{sapphire}}(T) = 4.5 \times 10^{-6} + 6.2(T + 273) \times 10^{-9}^\circ\text{C}^{-1}$ , and we found the strain value at around  $-1.8\%$ .

The calculated lattice mismatch between h-BN and underlying sapphire is 5.2%, which closely matches the measured value of 5.9% obtained from XRD by employing the Williamson–Hall method.<sup>35</sup> We performed the following calculation for obtaining the lattice mismatch and critical thickness,<sup>36</sup>

$$\varepsilon = \frac{2a_{\text{film}} - a_{\text{sub}}}{a_{\text{sub}}}, \quad (2)$$

$$h_c = \frac{b}{2\varepsilon \cos \phi} \left( 1 + \left( \frac{1 - \nu}{4\pi \cos^2 \lambda (1 + \nu)} \right) \ln \left( \frac{h_c}{b} \right) \right), \quad (3)$$

where  $\varepsilon$  denotes the lattice mismatch,  $a_{\text{film}}$  and  $a_{\text{sub}}$  are the lattice constants of h-BN thin films and sapphire substrates, respectively,  $h_c$  the critical thickness,  $\nu$  Poisson's ratio,  $b$  the magnitude of Burger's vector,  $\phi$  the angle between the slip plane and the strained interface normal, and  $\lambda$  the angle between the Burgers vector and the direction in the interface, normal to the dislocation line. Considering the in-plane lattice constants of h-BN and sapphire to be 2.5 and 4.76 Å, respectively, the calculated strain due to the lattice mismatch is 5.2%. Hence, the lattice mismatch between vdW h-BN and sapphire plays a significant role in inducing a compressive strain in the film. Considering Burger's vector to be  $\sqrt{2}a_{\text{film}}$  for square-octagon dislocation pairs and  $\phi = \lambda = 0^\circ$  for *a*-type dislocations, the critical thickness value of 3.93 Å can be obtained, indicating that the film is relaxed.

Another salient feature is the so-called "hillock" formation observed in the AFM data, which creates some degree of surface

roughness on the h-BN films. Films under biaxial stress do not relax uniformly and can create a potential gradient between relatively relaxed grains and the surrounding films. This causes a flow of the atoms along the interface of the film and substrate, and finally, the relaxed area grows out from the base as a hillock. Formation of hillocks, a random extrusion of film materials, is mostly controlled by grain boundary diffusion, interface diffusion, and lattice diffusion, respectively.<sup>37</sup> In a recent study, similar hillock-like features were reported as islands or debris on MOCVD-grown h-BN-on-sapphire, and their density was found to be a function of  $\text{NH}_3$  flux.<sup>38</sup> Although  $\text{NH}_3$  was not used during our growth, gas phase reactions of the borazine precursor can still produce particles or amino-borane oligomers. Formation of hillocks could be some kind of recrystallization or reconstruction of the grain structure. Hillocks may extract out of grains or grain boundaries due to the TEC mismatch between the films and the substrate, which could also produce wrinkles as described before.<sup>37</sup> The measured hillock height is in the range of 27–32 nm with a lateral coverage of 120–180 nm as shown in Fig. 4(d). It is likely that the hillocks are h-BN nanoparticles and fall randomly onto the substrate during growth. A large density of hillocks on the h-BN surface obstructs the formation of smooth thin films over a large area, and the roughness of the surface will limit further application of such films.

#### D. Raman study

Raman spectra of the as-grown sample are shown in Fig. 5(a). Several signature peaks at 378.6, 418.91, 430.6, 451, 577.2, and 749.6  $\text{cm}^{-1}$  are observed from the sapphire substrates. The peak at 1368  $\text{cm}^{-1}$  corresponds to the  $E_{2g}$  vibrational mode of h-BN and is analogous to the G peak in graphene.<sup>33</sup> This peak shifts to higher phonon frequencies compared to the bulk h-BN Raman peak at  $\sim 1366 \text{ cm}^{-1}$ , suggesting that our film is under strain.<sup>34</sup> Red and blue shifts in the Raman peak are mostly caused by the presence of compressive and tensile strain, respectively, in the films. The mismatch in TEC, leading to compressive strain in our sample, is also consistent with the results reported in Ref. 31. Moreover, this strain is biaxial since no splitting is observed.<sup>39</sup> In addition, the presence of the wrinkles, which is a consequence of compressive strain, also supports this statement. The experimentally measured Raman peak of the h-BN sample was fit to Lorentz functions, and the full width at half maximum (FWHM) was estimated to be 29.5  $\text{cm}^{-1}$  as shown in Fig. 5(b).

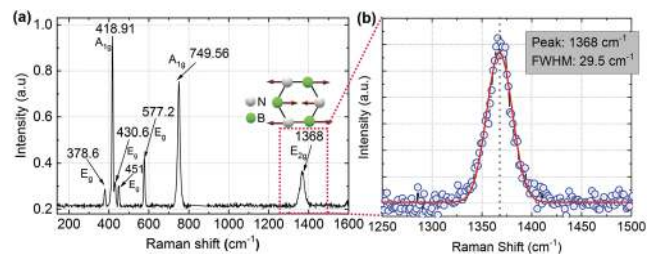


**FIG. 5.** (a) Raman spectra of h-BN films deposited on sapphire substrates, the perturbation corresponding to the  $E_{2g}$  phonon mode is shown as the inset, and (b) a close-up view of the  $E_{2g}$  Raman mode.

### E. TEM study

The atomic structure and stacking order of the as-grown h-BN multilayer films were further studied by cross-sectional HRTEM. Despite the lattice mismatch between h-BN and sapphire, a defect-free interface with a clear layered structure of h-BN can be seen in Fig. 6(a). The intermediate region between sapphire and h-BN is a buffer layer, which evolves perhaps due to the sapphire surface reconstruction upon h-BN growth in order to compensate the large lattice mismatch between h-BN and sapphire. Figure 6(b) shows the expanded view of the TEM image with the sapphire buffer layer after reconstruction at the growth interface. The BN interlayer spacing was measured to be  $\sim 0.332$  nm as shown in Fig. 6(c). This value is very close to the bulk h-BN with a spacing of  $\sim 0.33$  nm, suggesting almost no disordered stacking sequences of crystal planes.<sup>40</sup> This result also indicates the absence of t-BN or any other phases in the material, which strongly supports our XRD results. Figure 6(d) presents the measured 2D fast Fourier transform (FFT) pattern of the h-BN region.

The electron energy loss spectrum (EELS), shown in Fig. 6(e), exhibits two distinct absorption peaks at  $\sim 190$  and  $\sim 400$  eV, which correspond to the K-edge onsets for B and N, respectively. These absorption peaks further split and generate two closed-spaced peaks at the corresponding energy levels. Two low-energy peaks around 191 and 198 eV induced by the B-K edge spectra originate from  $\pi^*$  and  $\sigma^*$  states, respectively. The high-energy peaks at 403 and 410 eV at the N-K edge come from  $\pi^*$  and  $\sigma^*$  states, respectively. These fine structure spectra support the formation of  $sp^2$  hybridized h-BN films, suggesting that the material has a hexagonal layered structure.<sup>41</sup> This is also evident from our cross-sectional TEM image.

### F. XPS study

B 1s, N 1s, O 1s, and C 1s core-level spectra measured from the as-grown h-BN films by x-ray photoelectron spectroscopy (XPS) are shown in Fig. 7(a). The B 1s and N 1s core-level spectra occur due to several factors. The primary reason is the B–N bonding in

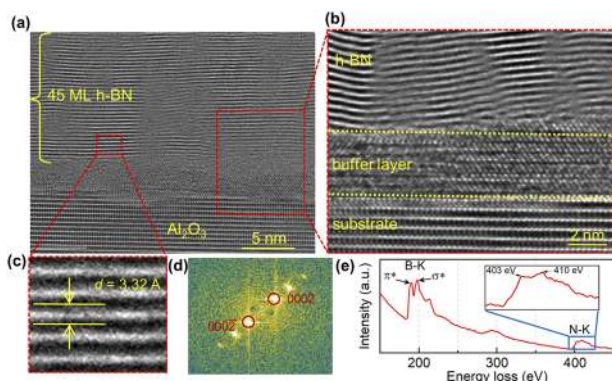


**FIG. 6.** (a) High-resolution cross-sectional TEM image of as-grown 45 ML h-BN films on sapphire, (b) expanded view of the image with the sapphire buffer layer after reconstruction at the growth interface, (c) lattice-spacing of h-BN, (d) FFT pattern of the h-BN cross section, indicating high crystallinity and quality, and (e) EELS spectra of h-BN films confirming  $sp^2$  bonding of h-BN.

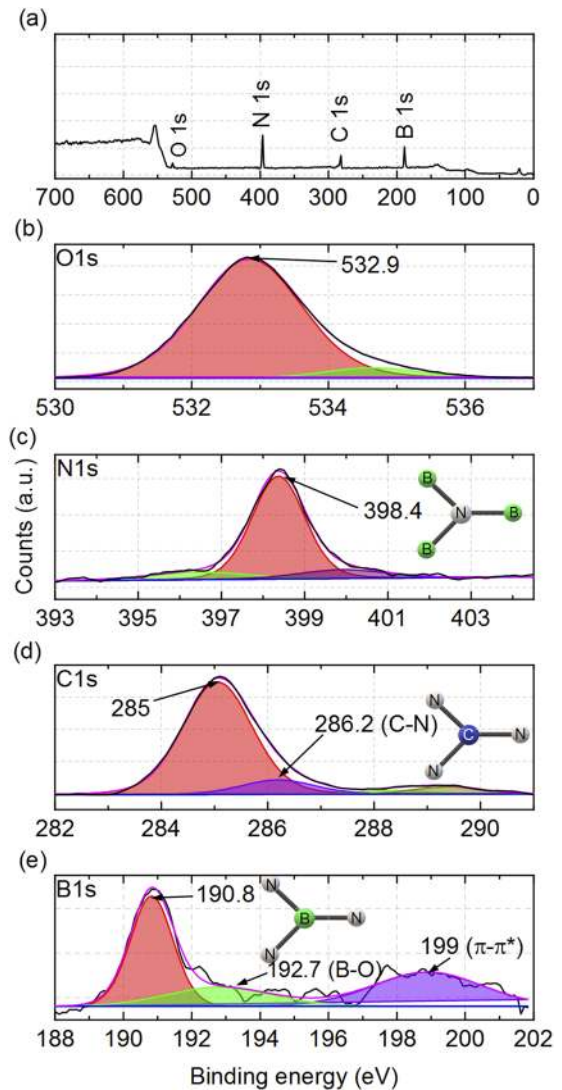


**FIG. 7.** (a) Survey XPS spectra; high resolution XPS spectra: (b) O 1s, (c) N 1s, (d) C 1s, and (e) B 1s of as-grown h-BN.

h-BN thin films, while other factors like N–N or B–N<sub>2</sub>–O bonding are also noteworthy and may be responsible for stable defects like nitrogen vacancies, substituted oxygen atoms in nitrogen sites, and self-interstitial N<sub>i</sub>. Gaussian–Lorentzian fitting was used to deconvolute the XPS peaks to extract the contribution of each element to the whole spectrum.

The weak O 1s peak found at 532.9 eV could be due to the presence of C–O or C=O species absorbed while transferring the sample to the XPS chamber as shown in Fig. 7(b).<sup>37</sup> The N 1s peak was found at the binding energy of 398.4 eV, which signifies the bonding between three boron atoms with one nitrogen atom as schematically shown in Fig. 7(c). These results are in good agreement with the reported values of B–N bonding, which is actually the bonding between three boron atoms with one nitrogen atom.<sup>42</sup>

The binding energy was calibrated with respect to the C 1s peak at 285 eV, as shown in Fig. 7(d). This peak value is very close to the binding energy of graphite but the FWHM of the peak is 1.57 eV, which is much higher than that of pure graphite (0.35 eV). We also obtain an additional peak at a higher energy of 286.2 eV due to the bonding of C with N, which has higher electronegativity than C.<sup>43</sup> Despite the use of a carbon-free precursor, we observed a very weak C 1s peak; these are possibly adventitious carbons. The bulk-like films on a non-carbon substrate eliminate the possibility of obtaining the C 1s peak and its associated C–N peak from any other sources except from the film itself.

The existence of bonding between one B atom with three N atoms was revealed at a binding energy of 190.8 eV, which is the B 1s peak as shown in Fig. 7(e) and is in good agreement with the previously reported results.<sup>44</sup> We also observed the shifting of the peak toward higher binding energies by an amount of 1.9 eV from the B–N bonding. This peak at higher energy (192.7 eV) is called a B–O peak, which occurs due to the higher electronegativity of the hydroxide anion compared to that of the nitrogen. Note that the  $\pi$ – $\pi^*$  plasmon shake-up peak was found at a peak around 199 eV.<sup>45</sup> The peak shifting and bonding analyses well define how N, B, O, and unintentional impurity carbon atoms are bonded with each other. The B/N ratio was found to be 0.98, which is indicative of stoichiometric composition.

#### IV. CONCLUSION

In summary, we have carried out systematic post-growth characterizations of CVD-grown h-BN thin films by XRD, AFM, SEM, Raman spectroscopy, TEM, and XPS measurements. Although the microscopic and spectroscopic characterization techniques used to identify material properties are routine, our comprehensive analysis of h-BN-on-sapphire reveals a new set of insights into the h-BN films. The underlying physics of the presence of wrinkles and residual strain within the films is rigorously studied, and our hypothesis is corroborated by these characterization results. Most importantly, the characterization results are shown for the films, which are grown using the carbon-free precursor “borazine.” Our systematic and comprehensive characterization studies of borazine-based h-BN are believed to bring many important material perspectives. The borazine precursor is essential since it minimizes the possibility of the presence of carbon impurities and shows a new way of achieving low-defect h-BN. This will eventually help develop single photon emitters through deterministic point defects. It turns out that the wrinkles on the films are a serious drawback with regard to using this approach for quantum information science applications. Therefore, our next step is to get around this wrinkle problem by transferring the films to SiO<sub>2</sub>/Si substrates by employing a polymer-material-free process.<sup>31</sup> Hence, CVD-grown h-BN transferred onto SiO<sub>2</sub>/Si substrates will reduce the strain, which will eventually pave the way toward the realization of wrinkle-free h-BN for achieving single-photon emission from deterministic point defects. It is expected that the outcome of our study has the potential to accelerate advancements in fundamental vdW material science, and it will facilitate a wide range of application areas, spanning over ultrawide-bandgap electronics, optoelectronics, sensing, and photonics.

#### ACKNOWLEDGMENTS

Sandia National Laboratories is a multimission laboratory managed and operated by National Technology and Engineering Solutions of Sandia, LLC, a wholly owned subsidiary of Honeywell International, Inc., for the U.S. Department of Energy's National Nuclear Security Administration under Contract No. DE-NA-0003525.

S.A. gratefully acknowledges funding by the AFRL Summer Faculty Fellowship Program, Contract No. FA9550-15-F-0001.

The authors wish to acknowledge the support of Dr. Tong Zhang and Campus Microscopy and Imaging Facility (CMIF) at OSU for SEM image processing.

The authors wish to thank Dr. Dan Gauthier at OSU, Dr. Darshana Wickramaratne at US Naval Research Laboratory, and Dr. Dipankar Chugh at ANU for many helpful discussions and several insightful comments.

#### DATA AVAILABILITY

The data that support the findings of this study are available from the corresponding author upon reasonable request.

#### REFERENCES

- Q. Cai, D. Scullion, W. Gan, A. Falin, S. Zhang, K. Watanabe, T. Taniguchi, Y. Chen, E. J. G. Santos, and L. H. Li, “High thermal conductivity of high-quality monolayer boron nitride and its thermal expansion,” *Sci. Adv.* **5**, eaav0129 (2019).
- W. Auwärter, “Hexagonal boron nitride monolayers on metal supports: Versatile templates for atoms, molecules and nanostructures,” *Surf. Sci. Rep.* **74**, 1–95 (2019).
- N. Kostoglou, K. Polychronopoulou, and C. Rebholz, “Thermal and chemical stability of hexagonal boron nitride (h-BN) nanoplatelets,” *Vacuum* **112**, 42–45 (2015).
- S. Lazić, A. Espinha, S. P. Yanguas, C. Gibaja, F. Zamora, P. Ares, M. Chhowalla, W. S. Paz, J. J. P. Burgos, and A. Hernández-Mínguez, “Dynamically tuned non-classical light emission from atomic defects in hexagonal boron nitride,” *Commun. Phys.* **2**, 113 (2019).
- Z. Liu, Y. Gong, W. Zhou, L. Ma, J. Yu, J. C. Idrobo, J. Jung, A. H. MacDonald, R. Vajtai, and J. Lou, “Ultrathin high-temperature oxidation-resistant coatings of hexagonal boron nitride,” *Nat. Commun.* **4**, 2541 (2013).
- J. Wang, F. Ma, W. Liang, and M. Sun, “Electrical properties and applications of graphene, hexagonal boron nitride (h-BN), and graphene/h-BN heterostructures,” *Mater. Today Phys.* **2**, 6–34 (2017).
- S. Ali and K. S. Thygesen, “V<sub>N</sub>C<sub>B</sub> defect as source of single photon emission from hexagonal boron nitride,” *2D Mater.* **7**, 031007 (2020).
- G.-D. Hao, M. Taniguchi, and S.-i. Inoue, “Highly deep ultraviolet-transparent h-BN film deposited on an Al<sub>0.7</sub>Ga<sub>0.3</sub>N template by low-temperature radio-frequency sputtering,” *Materials* **12**, 4046 (2019).
- C. Chen, J. Wang, D. Liu, C. Yang, Y. Liu, R. S. Ruoff, and W. Lei, “Functionalized boron nitride membranes with ultrafast solvent transport performance for molecular separation,” *Nat. Commun.* **9**, 1902 (2018).
- C. H. Lin, H. C. Fu, B. Cheng, M. L. Tsai, W. Luo, L. Zhou, S. H. Jang, L. Hu, and J. H. He, “A flexible solar-blind 2D boron nitride nanopaper-based photodetector with high thermal resistance,” *npj 2D Mater. Appl.* **2**, 23 (2018).
- S. Liu, R. He, Z. Ye, X. Du, J. Lin, H. Jiang, B. Liu, and J. H. Edgar, “Large-scale growth of high-quality hexagonal boron nitride crystals at atmospheric pressure from an Fe–Cr flux,” *Cryst. Growth Des.* **17**, 4932–4935 (2017).
- H. Jeong, D. Y. Kim, J. Kim, S. Moon, N. Han, S. H. Lee, O. F. N. Okello, K. Song, S. Y. Choi, and J. K. Kim, “Wafer-scale and selective-area growth of high-quality hexagonal boron nitride on Ni (111) by metal-organic chemical vapor deposition,” *Sci. Rep.* **9**, 5736 (2019).
- Y. Kobayashi and T. Akasaka, “Hexagonal BN epitaxial growth on (0001) sapphire substrate by MOVPE,” *J. Cryst. Growth* **310**, 5044–5047 (2008).

- <sup>14</sup>R. Page, J. Casamento, Y. Cho, S. Rouvimov, H. G. Xing, and D. Jena, "Rotationally aligned hexagonal boron nitride on sapphire by high-temperature molecular beam epitaxy," *Phys. Rev. Mater.* **3**, 064001 (2019).
- <sup>15</sup>T. S. Cheng, A. Summerfield, C. J. Mellor, A. N. Khlobystov, L. Eaves, C. T. Foxon, P. H. Beton, and S. V. Novikov, "High-temperature molecular beam epitaxy of hexagonal boron nitride with high active nitrogen fluxes," *Materials* **11**, 1119 (2018).
- <sup>16</sup>Y. Kobayashi, K. Kumakura, T. Akasaka, and T. Makimoto, "Layered boron nitride as a release layer for mechanical transfer of GaN-based devices," *Nature* **484**, 223–227 (2012).
- <sup>17</sup>K. Nakamura, "Preparation and properties of boron nitride films by metal organic chemical vapor deposition," *J. Electrochem. Soc.* **133**, 1120 (1986).
- <sup>18</sup>Y. Shi, C. Hamsen, X. Jia, K. K. Kim, A. Reina, M. Hofmann, A. L. Hsu, K. Zhang, H. Li, and Z.-Y. Juang, "Synthesis of few-layer hexagonal boron nitride thin film by chemical vapor deposition," *Nano Lett.* **10**, 4134–4139 (2010).
- <sup>19</sup>M. Chubarov, H. Pedersen, H. Högberg, V. Darakchieva, J. Jensen, P. O. Å. Persson, and A. Henry, "Epitaxial CVD growth of sp<sup>2</sup>-hybridized boron nitride using aluminum nitride as buffer layer," *Phys. Status Solidi RRL* **5**, 397–399 (2011).
- <sup>20</sup>A. Rice, A. Allerman, M. Crawford, T. Beechem, T. Ohta, C. Spataru, J. Figiel, and M. Smith, "Effects of deposition temperature and ammonia flow on metal-organic chemical vapor deposition of hexagonal boron nitride," *J. Cryst. Growth* **485**, 90–95 (2018).
- <sup>21</sup>G. Younes, G. Ferro, M. Soueidan, A. Brioude, V. Souliere, and F. Cauwet, "Deposition of nanocrystalline translucent h-BN films by chemical vapor deposition at high temperature," *Thin Solid Films* **520**, 2424 (2012).
- <sup>22</sup>S. Sonde, A. Dolocan, N. Lu, C. Corbet, M. J. Kim, E. Tutuc, S. K. Banerjee, and L. Colombo, "Ultrathin, wafer-scale hexagonal boron nitride on dielectric surfaces by diffusion and segregation mechanism," *2D Mater.* **4**, 025052 (2017).
- <sup>23</sup>J. Lu, P. S. E. Yeo, Y. Zheng, H. Xu, C. K. Gan, M. B. Sullivan, A. H. Castro Neto, and K. P. Loh, "Step flow versus mosaic film growth in hexagonal boron nitride," *J. Am. Chem. Soc.* **135**, 2368–2373 (2013).
- <sup>24</sup>A.-R. Jang, S. Hong, C. Hyun, S. I. Yoon, G. Kim, H. Y. Jeong, T. J. Shin, S. O. Park, K. Wong, and S. K. Kwak, "Wafer-scale and wrinkle-free epitaxial growth of single-orientated multilayer hexagonal boron nitride on sapphire," *Nano Lett.* **16**, 3360–3366 (2016).
- <sup>25</sup>J. C. Koepke, J. D. Wood, Y. Chen, S. W. Schmucker, X. Liu, N. N. Chang, L. Nienhaus, J. W. Do, E. A. Carrion, and J. Hewaparakrama, "Role of pressure in the growth of hexagonal boron nitride thin films from ammonia-borane," *Chem. Mater.* **28**, 4169–4179 (2016).
- <sup>26</sup>P.-C. Huang and M.-S. Wong, "Nanostructures of mixed-phase boron nitride via biased microwave plasma-assisted CVD," *Vacuum* **100**, 66–70 (2014).
- <sup>27</sup>K. Ahmed, R. Dahal, A. Weltz, J. J.-Q. Lu, Y. Danon, and I. B. Bhat, "Effects of sapphire nitridation and growth temperature on the epitaxial growth of hexagonal boron nitride on sapphire," *Mater. Res. Express* **4**, 015007 (2017).
- <sup>28</sup>Y. Kobayashi, T. Akasaka, and T. Makimoto, "Hexagonal boron nitride grown by MOVPE," *J. Cryst. Growth* **310**, 5048–5052 (2008).
- <sup>29</sup>R. Dahal, J. Li, S. Majety, B. N. Pantha, X. K. Cao, J. Y. Lin, and H. X. Jiang, "Epitaxially grown semiconducting hexagonal boron nitride as a deep ultraviolet photonic material," *Appl. Phys. Lett.* **98**, 211110 (2011).
- <sup>30</sup>J. Li, R. Dahal, S. Majety, J. Y. Lin, and H. X. Jiang, "Hexagonal boron nitride epitaxial layers as neutron detector materials," *Nucl. Instrum. Methods Phys. Res.* **654**, 417–420 (2011).
- <sup>31</sup>K. Bera, D. Chugh, A. Patra, H. H. Tan, C. Jagadish, and A. Roy, "Strain distribution and thermal strain relaxation in MOVPE grown hBN films on sapphire substrates," [arXiv:1907.05591](https://arxiv.org/abs/1907.05591) (2019).
- <sup>32</sup>X. Li, S. Sundaram, Y. El Gmili, T. Ayari, R. Puybaret, G. Patriarche, P. L. Voss, J. P. Salvestrini, and A. Ougazzaden, "Large-area two-dimensional layered hexagonal boron nitride grown on sapphire by metalorganic vapor phase epitaxy," *Cryst. Growth Des.* **16**, 3409–3415 (2016).
- <sup>33</sup>H. T. T. Nguyen, "Graphene layer of hybrid graphene/hexagonal boron nitride model upon heating," *Carbon Lett.* **29**, 521–528 (2019).
- <sup>34</sup>Q. Cai, D. Scullion, A. Falin, K. Watanabe, T. Taniguchi, Y. Chen, E. J. G. Santos, and L. H. Li, "Raman signature and phonon dispersion of atomically thin boron nitride," *Nanoscale* **9**, 3059–3067 (2017).
- <sup>35</sup>D. Nath, F. Singh, and R. Das, "X-ray diffraction analysis by Williamson-Hall, Halder-Wagner and size-strain plot methods of CdSe nanoparticles—A comparative study," *Mater. Chem. Phys.* **239**, 122021 (2020).
- <sup>36</sup>J. Yu, L. Wang, Z. Hao, Y. Luo, C. Sun, Y. Han, B. Xiong, J. Wang, and H. Li, "Theoretical study on critical thickness of heteroepitaxial h-BN on hexagonal crystals," *J. Cryst. Growth* **467**, 126–131 (2017).
- <sup>37</sup>K. Raić, "An explanation of hillock growth in thin Al films," *Surf. Eng.* **32**, 823–828 (2016).
- <sup>38</sup>X. Yang, S. Nitta, K. Nagamatsu, S.-Y. Bae, H.-J. Lee, Y. Liu, M. Pristovsek, Y. Honda, and H. Amano, "Growth of hexagonal boron nitride on sapphire substrate by pulsed-mode metalorganic vapor phase epitaxy," *J. Cryst. Growth* **482**, 1–8 (2018).
- <sup>39</sup>W. Pan, J. Xiao, J. Zhu, C. Yu, G. Zhang, Z. Ni, K. Watanabe, T. Taniguchi, Y. Shi, and X. Wang, "Biaxial compressive strain engineering in graphene/boron nitride heterostructures," *Sci. Rep.* **2**, 893 (2012).
- <sup>40</sup>M. Gao, J. Meng, Y. Chen, S. Ye, Y. Wang, C. Ding, Y. Li, Z. Yin, X. Zeng, and J. You, "Catalyst-free growth of two-dimensional hexagonal boron nitride few-layers on sapphire for deep ultraviolet photodetectors," *J. Mater. Chem. C* **7**, 14999–15006 (2019).
- <sup>41</sup>N. G. Chopra, R. J. Luyken, K. Cherrey, V. H. Crespi, M. L. Cohen, S. G. Louie, and A. Zettl, "Boron nitride nanotubes," *Science* **269**, 966–967 (1995).
- <sup>42</sup>Q. Wu, J. H. Park, S. Park, S. J. Jung, H. Suh, N. Park, W. Wongwiriyan, S. Lee, Y. H. Lee, and Y. J. Song, "Single crystalline film of hexagonal boron nitride atomic monolayer by controlling nucleation seeds and domains," *Sci. Rep.* **5**, 16159 (2015).
- <sup>43</sup>M. R. Uddin, T. C. Doan, J. Li, K. S. Ziemer, J. Y. Lin, and H. X. Jiang, "Electrical transport properties of (BN)-rich hexagonal (BN)C semiconductor alloys," *AIP Adv.* **4**, 087141 (2014).
- <sup>44</sup>M. R. Uddin, S. Majety, J. Li, J. Y. Lin, and H. X. Jiang, "Layer-structured hexagonal (BN)C semiconductor alloys with tunable optical and electrical properties," *J. Appl. Phys.* **115**, 093509 (2014).
- <sup>45</sup>M. S. Bresnehan, M. J. Hollander, M. Wetherington, K. Wang, T. Miyagi, G. Pastir, D. W. Snyder, J. J. Gengler, A. A. Voevodin, and W. C. Mitchell, "Prospects of direct growth boron nitride films as substrates for graphene electronics," *J. Mater. Res.* **29**, 459–471 (2014).